International Journal of Nanomedicine

Dovepress

open access to scientific and medical research

Open Access Full Text Article

ORIGINAL RESEARCH

ROS-responsive Galactosylated-nanoparticles with Doxorubicin Entrapment for Triple Negative Breast Cancer Therapy

Jingyi Zhou*, Kangkang Li*, Xinlong Zang, Yi Xie, Jinxiao Song, Xuehong Chen

School of Basic Medicine, Qingdao University, Qingdao, People's Republic of China

*These authors contributed equally to this work

Correspondence: Xinlong Zang; Xuehong Chen, Email zangxinlong@126.com; chenxuehong@qdu.edu.cn

Background: Triple negative breast cancer (TNBC) is one of the most aggressive tumors with high metastasis and mortality, which constitutes 15~20% of all breast cancers. Chemotherapy remains main therapeutic option in the treatment of patients with TNBC.

Methods: We developed reactive oxygen species (ROS)-responsive galactosylated nanoparticles (DOX@NPs) as an efficiently targeted carrier for doxorubicin (DOX) delivery to inhibit the growth of TNBC in vitro and in vivo. DOX@NPs were composed of polyacrylate galactose and phenylboronic derivatives conjugation. The in vitro cytotoxicity, cellular uptake, cell apoptosis and cycle distribution of tumor cells treated with different formulations were investigated. Meanwhile in vivo biodistribution and antitumor effects were investigated in a 4T1 tumor-bearing mouse model.

Results: DOX@NPs showed good ROS responsiveness and rapid DOX release in the presence of H_2O_2. Furthermore, our data suggested that DOX@NPs could effectively trigger tumor cells apoptosis and cycle arrest, efficiently accumulate into tumor sites, and suppress tumor growth without adverse side effects.

Conclusion: Our results suggested DOX@NP with potent potential as a promising nanocarrier for TNBC therapy, which deserved further investigation for other cancer treatment.

Keywords: triple negative breast cancer, doxorubicin, ROS-responsive, drug delivery

Introduction

Breast cancer is the leading cause in female-related tumors in 2022, which affects 12% of women in the world. Among these types, triple negative breast cancer (TBNC) characterized with the absence of estrogen receptor (ER), progesterone receptor (PR) and human epidermal growth factor receptor 2 (HER-2), is one of the most aggressive tumors with high metastasis and poor survival.[1] Recent decades have witnessed the understanding of mechanisms and the development of effective antitumor strategies against TNBC.[2–7] However, chemotherapeutic drugs, such as doxorubicin (DOX) and paclitaxel (PTX), remain one of main treatment options for TNBC. Unfortunately, chemotherapeutic agents are restricted as a result of poor solubility, short circulation time, nonselective distribution, drug resistance and severe side effects. More importantly, repeated and high doses of chemotherapeutics can cause severe damages such as cardiotoxicity and immunosuppression.[8] Herein, it is imperative to develop a targeted delivery system for TNBC therapy. Fortunately, versatile nanoparticle-based drug delivery systems, polymers, dendrimers, liposomes, and inorganic nanoparticles, have been exploited as a promising approach to improve the original pharmaceutical and pharmacological effects of these drugs.[9] For example, Haggag et al designed a liposomal nanocarriers for codelivery Ran-RCC1 inhibitory peptide and DOX, which demonstrated high tumor accumulation and antitumor effects in tumor-bearing mice.[3] Guanabenz acetate-loaded polymersome displayed significant improvements in cellular uptake and cytotoxicity to MDA-MB-231 and MCF-7 cells compared to free drug, resulting in tumor regression in vivo.[2] Furthermore, a number of nanoparticle-based

Received: 21 November 2022
Accepted: 7 March 2023
Published: 22 March 2023

delivery systems against tumor are in clinical and preclinical trials and some of them, such as Doxil® and Taxol®, have been approved by the US Food and Drug Administration (FDA) for TNBC therapy.[10]

Carbohydrate functionalized nanoparticles have served as multivalent scaffolds to carry various payloads, including small molecular drugs, nucleic acids, peptides and proteins and even quantum dots, and other nanoparticles.[11] Through receptor-ligand interactions, these glycol-materials have been shown the potential in mediating various biological activities such as immune response and intercellular communications.[12] Furthermore, the ideal nanocarrier should address the requirements of prolonged circulation time, controlled payload release and nontoxic degradation products. Glycol materials, including natural hyaluronic acid, dextran and cellulose and synthetic carbonate conjugations like galactose, mannose, glucose derivatives, possess excellent properties of hydrophilicity, degradability, and biocompatibility without serious toxicity and immunogenicity.[13] For example, Qiu et al developed pH-responsive micelles composed of hyaluronic acid conjugated to poly (L-histidine) (HA-Phis) for intracellular DOX delivery.[14] HA-Phis formed stable micelles in aqueous solutions and exhibited high cytotoxicity and internalization in MCF-7 cells, which was attributed to that HA could serve as hydrophilic shell and interact with overexpressed CD44 receptors.[15] Nevertheless, most natural saccharides are linear polymers only carrying limited modified sites, accompanied with their initial water-solubility, making it difficult for further functional modification. Polymeric acrylate derivatives are relatively easy to be functionalized with inherent biocompatibility and stimuli-responsivity.[16] For instance, Piloni et al designed and synthesized ABC triblock terpolymer based on methyl acrylate glucose, mannose and galactose via reversible addition-fragmentation chain-transfer (RAFT) polymerization. These polymers could self-assemble into nanoparticles which were supposed to help targeting specific cell lines.[17] Herein, polyacrylate with pendent galactose is synthesized and then explored as a drug carrier.

To obtain intracellular drug release, nanoparticles that can respond to tumoral stimuli such as low pH, enzymes, glutathione (GSH) and reactive oxygen species (ROS), have been extensively explored.[18] Among these aforementioned stimuli, the relative high concentration of reactive oxygen species (ROS), including but not limited to hydrogen peroxide (H_2O_2), is a common feature in tumor cells and has been exploited to realize controllable release.[19] Typically, boronic esters are emerging ROS-cleavable groups that have been utilized to construct stimuli-responsive nanocarriers. Pei et al reported that yolk-shell nanoplatform containing boronic ester has been used for ROS-dependent cytochrome C and DOX delivery.[20] On the basis of a similar activation mechanism, Shao et al conjugated 4-hydroxymethyl-pinacol phenylborate to chitosan to encapsulate indocyanine green, which could be cleaved in response to ROS production.[21] These studies highlighted the potential of boronic ester for drug delivery and controlled release, which is expected to improve the efficiency and reliability of nanomedicines for tumor treatment.

In this study, we reported a smart nanocarrier (DOX@NPs) for delivering hydrophobic DOX to tumor cells, which could realize accelerated release in response to intracellular excessive ROS (Figure 1). The nanocarrier was composed of polyacrylate galactose (MAGlaOH) and phenyboronic (MAPBP) derivatives through RAFT polymerization, which could assemble into ROS-responsive nanoparticles (NPs) for DOX entrapment.[19] In vitro and in vivo studies were performed to investigate the physicochemical properties and tumor targeting and inhibition of resultant nanoparticles. Our results implied that DOX@NPs could effectively induce tumor cells apoptosis and cycle arrest, suppress tumor growth without adverse side effects, suggesting the potential of the nanoparticles as a promising nanocarrier for TNBC therapy.

Materials and Methods

Materials and Cell Culture

Hydroxyethyl methacrylate, TEA and boron trifluoride diethyl etherate were purchased from MACKLIN (Shanghai, China). Doxorubicin and beta-D-galactose pentaacetate were obtained from Energy Chemical (Shanghai, China). (Hydroxymethyl) phenylboronic acid pinacol ester, 2,2′-azobis(2-methylpropionitrile) (AIBN, 99%), methacryloyl chloride and 2-(dodecylthiocarbonothioylthio)-2-methylpropionic acid were purchased from Aladdin (Shanghai, China). Dialysis bag MD34 (3500 Da) was obtained from Solarbio (Beijing, China). DiR were purchase from MeilunBio (Suzhou, China). MTT solution, 2% phosphotungstic acid and 4′,6-diamidino- 2-phenylindole (DAPI) were obtained from Solaibio (Shanghai, China).

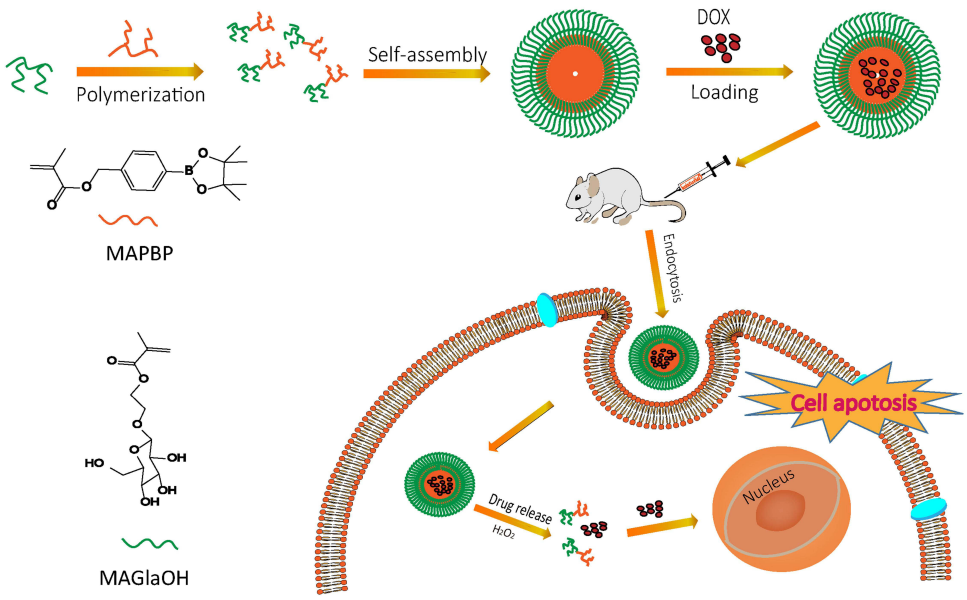

Figure 1 Schematic illustration of DOX@NPs antitumor responses. The copolymer was composed of polyacrylate derivatives, MAGlaOH and MAPBP, which could self-assemble to form nanoparticles with DOX driven by hydrophobic interactions. After systemic administration, DOX@NPs demonstrated tumor-specific accumulation and cellular uptake in tumor cells. Meanwhile intracellular excessive ROS triggered DOX release, which successively suppressed TNBC growth.

Female mouse 4T1 cells and human breast cancer MDA-MB-231 cells were obtained from American Type Culture Collection (ATCC, USA) and cultured in complete RMPI 1640 medium with 10% fetal bovine serum (FBS) and 1% penicillin-streptomycin. HUVEC were obtained from ATCC and maintained in HUVEC special culture medium (Procell, Wuhan, China) supplemented with 10% FBS and 1% penicillin/streptomycin. The cells were passaged by mechanical dissociation every two days and further cultured in a humidified incubator with 5% CO_2 at 37°C.

Synthesis and Characterization of Copolymers

Synthesis of MAGlaAc

2-Hydroxyethyl methacrylate (2.33 mL, 0.019 mol) was dissolved with β-D-galactose pentaacetate (5.0 g, 0.013 mol) in anhydrous dichloromethane (20 mL) under N_2 atmosphere, followed by the addition of hydroxy-methyl-phenylboronic pinacol ester (4.4 mL, 0.034 mol) drop-wise in ice bath. After stirring for 1 h at 0°C, the reaction was transferred to 25°C for another 18 h. The mixture was washed with deionized water (100 mL×2) and brine (100 mL×1) and dried with Mg_2SO_4. The organic solvent was concentrated under reduced pressure and residual was then purified by silica column chromatography (dichloromethane: ethyl acetate=4:1, v/v). MAGlaAc (4.4 g, 73% yield) was obtained as a light-yellow oil.

Synthesis of MAPBP

A solution of (4-(4,4,5,5-tetramethyl-1,3,2-dioxaborolan-2-yl) phenyl) methanol (5.85 g, 25 mmol) was added with TEA (3.05 g, 30 mmol) into anhydrous dichloromethane (30 mL). After cooling to 0°C, methacrylic chloride (2.7 g, 30 mmol) was added drop-wise into above solution within 1 h and then the system was warmed to room temperature and stirred for 10 h. After removing the solvent, the crude product was re-dissolved in ethyl acetate, washed with brine (50 mL×3), dried with Mg_2SO_4 and finally purified by silica column with petroleum ether/ethyl acetate (30:1, v/v). MAPBP (6.84 g, 80% yield) was obtained as a colorless solid.

Synthesis of PGlaAC

A mixture of 2-methyl-2-[(dodecylsulfanylthiocarbonyl) sulfanyl] propanoic acid (31.6 mg, 0.087 mmol), MAGlaAC (1 g, 2 mmol) and AIBN (2.86 mg, 0.017 mmol) were added separately into a round-bottom flask equipped with DMF (3 mL). The reaction system was then degassed and purged with N_2 three times, and performed at 75°C for 24 h. The

mixture was stirred at room temperature and dialyzed against deionized water for 24 h. After lyophilization, PGlaAC (0.83 g, 77% yield) was obtained as a light-yellow solid.

Synthesis of PGla-PPBP

PGlaAC (0.45 g, 0.11 mmol), MAPBP (0.42 g, 1.4 mmol) and AIBN (2.86 mg, 0.017 mmol) were placed in a round-bottom flask equipped with DMF (3 mL). The reaction was performed as described above. The products were dialyzed against deionized water for 24 h and lyophilized to obtain PGlaAC-PPBP (0.65 g, 75% yield) as a light-yellow solid. PGlaAC-PPBP (0.65 g, 0.1 mmol) was dissolved into anhydrous dichloromethane (30 mL), followed by adding dropwise of MeONa (30% in MeOH, 1 mL) at 0°C. The precipitates occurred and 1M HCl was added slowly to adjust pH=7.0. After dialysis and lyophilization, PGla-PPBP (0.5 g, 77% yield) was obtained as a light-yellow solid.

Preparation of DOX-loaded ROS-responsive Nanoparticles

DOX loaded ROS-responsive nanoparticles were prepared using a conventional dialysis method.[22] Briefly, 20 mg PGla-PPBP and 2 mg DOX were dissolved in DMSO and dialyzed against distilled water at room temperature for 24 h. The dialysis medium was changed every three hours. The nanoparticles were filtered through a 0.22 μm filter to obtain DOX@NPs. Similarly, DiR loaded nanoparticles were prepared as DiR@NPs.

Hemolytic Activity of ROS-responsive Nanoparticles

The hemolytic activity of PGla-PPBP nanoparticles was investigated using rabbit red blood cells. Briefly, 2 mL of fresh rabbit blood was added in a heparin-containing anticoagulant tube, which was diluted by PBS at a final concentration of 10% red blood cells (RBC) before use. The PGla-PPBP nanoparticles with different concentrations were incubated with equivalent RBCs for 4 h in a 37°C water bath.

Characterizations of DOX Loaded ROS-responsive Nanoparticles

The hydrodynamic sizes and zeta potential of the nanoparticles were evaluated using dynamic light scattering (DLS) technique (Malvern Nano-ZS device, UK) in triple. As for stability investigation, the nanoparticles were incubated with 10% FBS at room temperature and their particle size was measured using DLS technique as mentioned above. The morphology was observed under transmission electron microscope (TEM, JEM-2100Plus, Japan). In brief, the nanoparticles were dropped onto copper mesh, stained using 2% Phosphotungstic acid 44-hydrate (PTA) and imaged using TEM.

Encapsulation Efficiency of DOX@loaded Nanoparticles

The encapsulation (EE) and drug loading efficiency (DL) of DOX into nanoparticles were investigated using fluorescence spectrometry as previous reports.[23,24] DMSO was added into the nanoparticles suspensions to destroy the structures and then the concentration of DOX was determined in triplicate with $\lambda_{excitation}$=485 nm and $\lambda_{emission}$=585 nm using a microplate reader (BIOTEK, ELX-800, USA). The EE and DL were then calculated by the following formulas:

$$\text{EE } (\%) = \frac{\text{Weight of loaded DOX}}{\text{Weight of feeding DOX}} \times 100\%$$

$$\text{DL } (\%) = \frac{\text{Weight of loaded DOX}}{\text{Weight of loaded DOX and copolymers}} \times 100\%$$

ROS Responsiveness Evaluation

To investigate the ROS responsiveness, DOX@NPs was incubated with varying concentration of H_2O_2 (0–50 mM) for 2 h.[25,26] The particle sizes were determined using DLS technique as mentioned above. Furthermore, the morphological changes of nanoparticles treated with H_2O_2 were observed and captured by TEM.

In vitro Release of DOX@NPs

Dialysis method was used to investigate in vitro release behavior of DOX@NPs in the presence or absence of H_2O_2. Briefly, different DOX formulations were introduced into a dialysis bag (3500 Da, MWCO) and immersed into 50 mL PBS buffer (0.01 M, pH=7.4) with or without 1 mM H_2O_2 in shaker incubation at 37°C. At desired intervals, 5 mL samples were collected and replenished with fresh medium. DOX concentration was determined by the same method as mentioned above and all measurements were conducted in triplicate.

In vitro Cellular Uptake

Cellular uptake of free DOX and DOX@NPs was assessed in human MDA-MB-231 and murine 4T1 cells by flow cytometry analysis and Confocal Laser Scanning Microscope (CLSM). 1×10^6 cells MDA-MB-231 and 4T1 cells were seeded into six-well plates and further cultured overnight. DOX formulations (free DOX and DOX@NPs) were incubated with tumor cells for 4 h. After removing the culture medium, tumor cells were trypsinized, harvested and analyzed by flow cytometry.

For CLSM observation, 3×10^5 tumor cells were seeded into confocal culture dish and cultured for 24 h. The culture medium was then replenished with fresh medium containing 10 μg/mL free DOX or DOX@NPs and incubated for another 4 h. Subsequently, tumor cells in confocal culture dish were washed with PBS and fixed with 4% paraformaldehyde for 15 min. The nuclei were stained with DAPI and the dishes were washed with PBS three times. The images were obtained with CLSM (Axio-Imager LSM-800, Germany).

In vitro Cytotoxicity Assay

MTT assay was used to investigate the cytotoxicity of different DOX formulations to tumor cells. In brief, MDA-MB-231, 4T1 cells and HUVEC cells were seeded into 96-well plate at a density of 3×10^4 cells/well and cultured for 24 h. The medium was replenished with 100 μL fresh medium containing free DOX and DOX@NPs at the concentration of 0–10 μg/mL. After 24 or 48 h incubation, 10 μL MTT solution was added and further incubated for another 4 h. Formazan crystal was dissolved in 150 μL DMSO and the absorbance at 570 nm was measured using a microplate reader (BIOTEK, ELX-800, USA). Cell viability was calculated using the following equation and IC_{50} value was by GraphPad Prism software.

$$\text{Cel viability } (\%) = \frac{A_{\text{treated}} - A_{\text{blank}}}{A_{\text{control}} - A_{\text{blank}}} \times 100\%$$

In vitro ROS Evaluation in Tumor Cells

ROS generation was assessed using a reactive oxygen detection kit (DCFH-DA). Briefly, 4T1 and MDA-MB-231 cells were seeded into a 96-well plate at a density of 3×10^4 cells/well and cultured for 24 h. Tumor cells were co-incubated with blank NPs, free DOX and DOX@NPs at a DOX concentration of 5 μg/mL and blank NPs concentration of 50 μg/mL. After 24 h, cell culture medium was replaced and DCFH-DA (100 μL/well) solution was added and co-incubated for 30 min. Tumor cells were washed with PBS solution three times to remove the free DCFH-DA. Next, the fluorescence intensity was measured at 488 nm excitation and 525 nm emission by a fluorescence spectrophotometer (BioTek, ELX-800, USA).

Cell Apoptosis and Cycle Assay

The in vitro capability of DOX@NPs to induce apoptosis was evaluated through externalization of phosphatidyl serine using standard annexin V-FITC/PI staining. Briefly, 3×10^5 cells MDA-MB-231 and 4T1 cells were seeded into six-well plates and further cultured for 24 h to allow cell attachment. Continuously, free DOX and DOX@NPs were added into the wells at concentration of 5 or 10 μg/mL, respectively. After 12 h incubation, tumor cells were harvested followed by annexin V-FITC/PI staining, which was subjected to flow cytometry.

For cell cycle distribution investigation, MDA-MB-231 and 4T1 cells with and without exposure to free DOX or DOX@NPs were incubation for 12 h. Tumor cells were then trypsinized, harvested suspended in PBS and fixed with

70% ethanol. Cells were stained with Cell Cycle and Apoptosis Analysis Kit (Beyotime, Shanghai, China) and analyzed using CytoFLEX flow cytometry (Beckman Counter, USA).

In vivo Imaging

To investigate the biodistribution and antitumor effect of DOX formulations, a mouse model of 4T1 breast cancer was established. Female Balb/c mice with body weight of 20–22 g were obtained from PengYue company (Jinan, China). Ethics approval was obtained from Qingdao University Animal Studies Committee. All procedures involving animals were conducted with the guidelines of the Institutional Animal Care and Use Committee (IACUC) of Qingdao University.

To establish tumor orthotopic model, 1×10^6 4T1 cells suspended in 100 μL PBS buffer were subcutaneously seeded into the right mammary pads.[27] When the tumor sizes reached about 100 mm^3, the mice were intravenously administrated with DiR@NPs and fluorescence distribution was monitored using FX Pro In Vivo Imaging System (Carestream Molecular Imaging, Ontario, CA, USA). The mice were sacrificed and organs and tumor tissues were collected and observed after 48 h administration.

In vivo Antitumor Effect

To evaluate the anticancer effects of DOX formulations in vivo, mice bearing the 4T1 tumor were randomly separated into five groups (n=5 per group) and administrated with saline, low and high dosage DOX and DOX@NPs via tail vein. The injections were conducted every two days on fifth day after tumor inoculation. The body weight and tumor diameter were measured every two days. The tumor volume was calculated by the following equation. At the end of the experimental procedures, mice receiving different treatments were sacrificed to harvest tumor tissues that were weighed and fixed in 4% paraformaldehyde for histological evaluation.

$$\text{Tumor volume } (mm^3) = \frac{\text{the longest diamerter } \times \text{the shortest diamerter}^2}{2}$$

H&E Staining and Ki67 Assay

To evaluate histological changes, the obtained tumor tissues were embedded into paraffin and cut into 4 μm sections, followed by standard hematoxylin and eosin (H&E) staining. Furthermore, Ki67 immunohistochemistry (IHC) staining was performed in order to analyze the proliferation status.[28] The histological changes of organs were also evaluated using H&E staining as shown above. All the experiments were performed according to manufactures' instructions. These sections were then observed and imaged by Ti2-U Microscope (NIKON, Japan).

Serum Biochemical Analysis

At the end of the experiment, mice were sacrificed and blood samples (PBS, L-DOX, H-DOX, L-DOX@NPs and H-DOX@NPs) were collected by intracardiac puncture. Then, the plasma samples were obtained by centrifugation (5000 rpm, 4°C, 30 min), and the levels of aspartate aminotransferase (AST), blood urea nitrogen (BUN), creatine kinase (CK) and lactate dehydrogenase (LDH) were measured using Cobas 6000 automatic biochemical analyzer (Roche, Switzerland).

Statistical Analysis

All experimental analysis was performed in triplicate and all data were shown as mean ± standard deviation (SD). One-way ANOVA and two-tailed Student's *t*-test were used to determine statistical differences. $P<0.05$ was considered to have statistical significance.

Results and Discussion

Characterization of PGla-PPBP

The PGla-PPBP copolymer was synthesized by RAFT using trithiocarbonate as an initiator while MAGlaAc and MAPBP as hydrophilic and hydrophobic blocks.[29] The synthesis routes and typical ^{1}H NMR spectra of the PGla-PPBP block copolymers

are illustrated in Figures 2 and 3. All chemical shifts were expressed in parts per million (δ) relative to the tetramethylsilane signal. As shown in Figure 3B–E, the representative peaks of PGlaAC-PPBP appear at δ_l=7.7 and δ_m=6.8 (phenyl), $\delta_{f\text{-}h}$=4.48–5.31 (galactose), $\delta_{c\text{-}d}$=3.93–4.2 (-CH_2CH_2-), δ=1.96 (-OAc), δ_n=1.25 (-CH_3) and δ_k=0.75–1.2 (-CH3, -$(CH_2)_{10}CH_3$). As

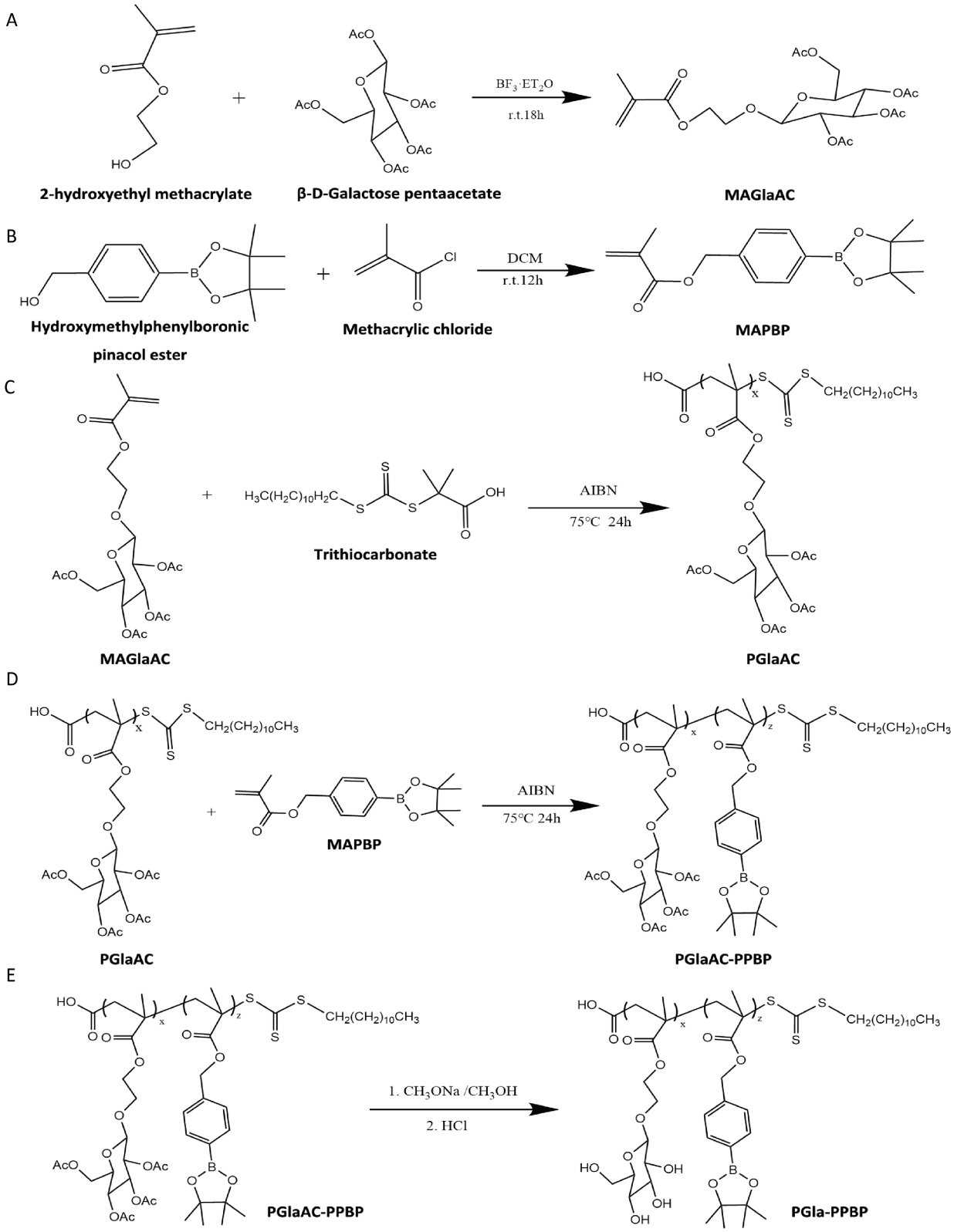

Figure 2 Synthesis route of PGla-PPBP copolymer. (**A**) MAGlaAc. (**B**) MAPBP. (**C**) PGlaAC. (**D**) PGlaAC-PPBP. (**E**) PGla-PPBP.

opposed to the spectrum in Figure 3A, the disappearance of peaks at δ=1.96 demonstrated the deprotection of acetoxyl group, indicating the successful synthesis of PGla-PPBP copolymer.

Intravenous administration is the mostly used route for nanomedicines in cancer treatment and therefore the hemolysis induced by nanoparticles should be of concern.[30] As shown in Figure 3F, PGla-PPBP nanoparticles had no obvious hemolysis at each tested concentration, showing good safety for intravenous injection.

Characterization of DOX@NPs

PGla-PPBP is an amphiphilic molecule which can form nanoparticles in aqueous solution. PGla is hydrophilic saccharides that can form outer shell, meanwhile hydrophobic drugs such as PTX and DOX can be entrapped into PPBP formed core through hydrophobic interactions. The DOX@NPs were prepared using dialysis method and their characterization features were shown in Figure 4 and Table 1. The mean diameter of blank nanoparticles was around 100 nm and zeta

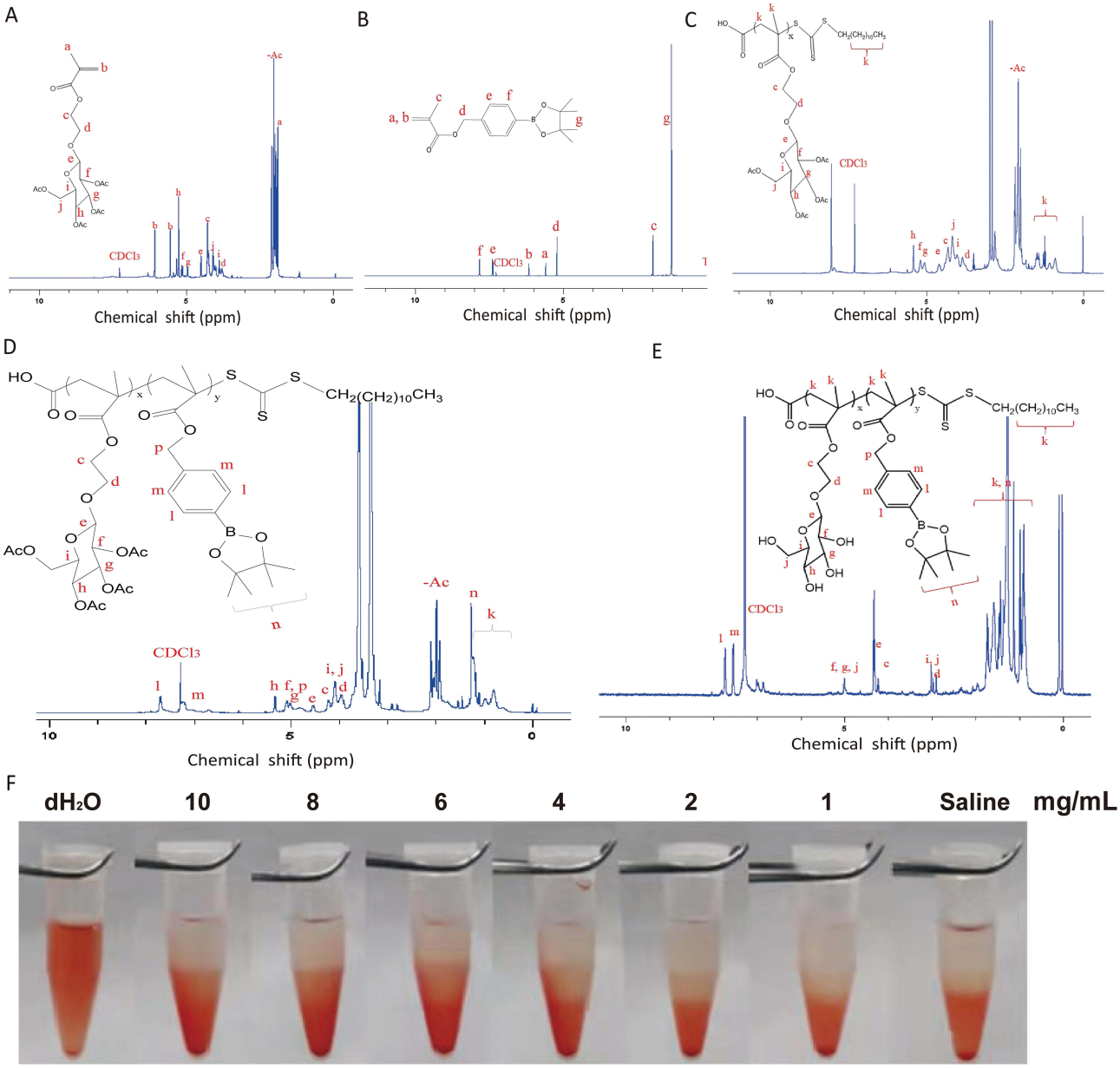

Figure 3 Characterization of PGla-PPBP copolymer. ^{1}H NMR spectrum of MAGlaAc (**A**), MAPBP (**B**), PGlaAC (**C**), PGlaAC-PPBP (**D**) and PGla-PPBP (**E**). (**F**) Hemolytic activity of PGla-PPBP nanoparticles.

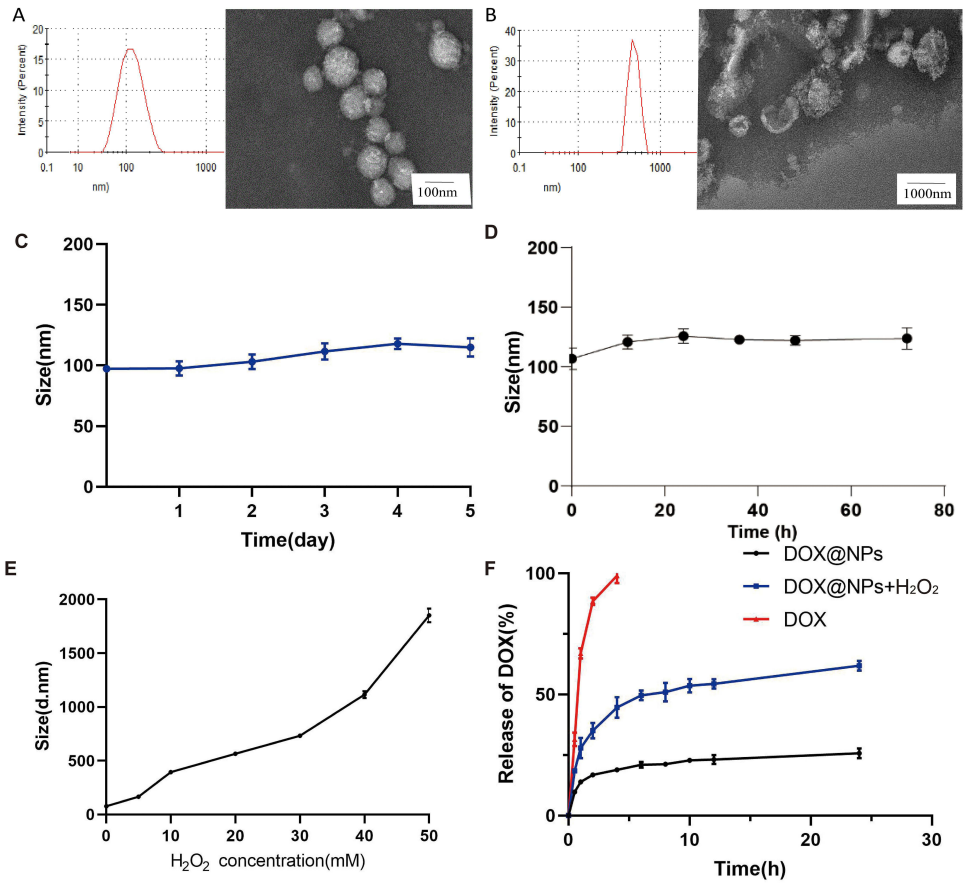

Figure 4 Characterizations of DOX@NPs. (**A**) Size distribution and TEM images of DOX@NPs. The bar shown is 100 nm. (**B**) Size distribution and TEM images of nanoparticles following H_2O_2 treatment. The bar shown is 100 nm and 1000 nm. Size changes of DOX@NPs in PBS (**C**) and after 10% FBS incubation (**D**). (**E**) Size change of DOX@NPs following different concentrations of H_2O_2 treatment as determined by DLS. (**F**) In vitro DOX release from DOX@NPs with 1 mM H_2O_2.

potential was about −12.1 mV. The introduction of DOX into the nanoparticles displayed slight increase in diameter but less than 15 nm. To investigate the physiological stability of DOX@NPs, the particle sizes were monitored in PBS for 5 days and the result was shown in Figure 4C. The mean diameter showed a slight tendency to increase during this period but less than 9 nm. Moreover, there was a slight increase (~17 nm) in particles sizes after incubation with 10% FBS (Figure 4D). The zeta potential of the nanoparticles is within the range from −12 mV to −8 mV, which might be attributed to a dynamic self-assembly process of the nanoparticles.[31] These data indicated the satisfactory stability of the nanoparticles in physiological environment. The small particle size and good stability are beneficial for their accumulation into tumor site through enhanced permeability and retention (EPR) effect. While the negative zeta potential was attributed to the saccharide shell, which can avoid the nanoparticles being quickly cleared in circulation.[32] Transmission electron microscopy (TEM) results revealed the nanoparticles with homogeneous size distribution and spherical morphology without obvious aggregation, in accordance with measurements using DLS technique. Subsequently, the encapsulation (EE) and drug loading efficiency (DL) of DOX in the nanoparticles have been determined using

Table 1 Characterization of DOX Loaded Nanoparticles

	Particle Sizes (nm)	PDI	Zeta Potential (mV)	EE (%)	DL (%)
Blank NPs	99.76	0.166	−12.1		
DOX@NPs	113.1	0.136	−16.4	56.38	4.29

fluorescence spectrum method. As shown in Table 1, the EE and DL were 56.38% and 4.29%, respectively, indicating the potential of the nanoparticles to encapsulate hydrophobic cargo such as DOX.

The ROS-responsive properties of the nanoparticles were evaluated using size and morphology in the presence of H_2O_2 conditions.[18] As shown in Figure 4B and E, the presence of H_2O_2 led to increased mean diameter in a concentration dependent manner. TEM images confirmed the disassemble the nanoparticles at the concentration of 4 mM H_2O_2 after 4 h incubation. The release behavior of DOX from DOX@NPs was also investigated in the presence or absence of H_2O_2 at 37°C (Figure 4F). Free DOX was rapidly diffused across the dialysis bag with more than 98% released into medium within 4 h. However, DOX release from DOX@NPs was in a controlled and sustained manner (<20% within 24 h) whereas the presence of 1 mM H_2O_2 significantly improved drug release, showing 60% release at 24 h. These results indicated the stability of DOX@NPs in physiological conditions, which could disassemble and payload release in response to ROS such as H_2O_2.

Cellular Uptake

A major requirement for antitumor effects of chemotherapeutic agent is determined by cellular uptake in tumor cells, which was evaluated using flow cytometry and confocal laser scanning microscopy (CLSM) in this study.[8] Figure 5 showed that a stronger DOX fluorescence signal was present in both MDA-MB-231 and 4T1 cells with prolonged incubation time, indicating a time-dependent internalization of free DOX and DOX@NPs. Free DOX revealed a high cellular uptake in both tumor cells due to the interactions between cationic DOX and negative plasma membrane. However, the complicated physiological and tumor microenvironment would absolutely reduce antitumor efficacy of free DOX as short circulation time, poor tumor distribution, drug resistance, and immunosuppression.[33] Therefore, various nanoplatforms have been developed to enhance the tumor-specific accumulation, cellular uptake and intracellular release of chemotherapeutics while decrease its efflux, nonspecific distribution and systemic toxicity.[34] The entrapment of DOX into PGla-PPBP nanoparticles could significantly improve cellular uptake in 4T1 cells, 2-fold than that of free DOX after 4 h incubation. Cellular uptake in MDA-MB-231 cells showed a similar tendency, in which DOX@NPs increased three times compared to free DOX after 4 h incubation. These findings confirmed the capability of enhanced DOX delivery to 4T1 and MDA-MB-231 cells by PGla-PPBP nanoparticles, though some studies showed higher free DOX internalization than nanomedicines due to positive charge of free DOX.[35]

The cellular uptake of DOX@NPs in breast cancer cells was visualized using CLSM. In agreement with flow cytometry results, fluorescence signal of DOX@NPs in both tumor cells presented a significant improvement than that of free DOX. In addition, the red fluorescence of DOX mainly located in the nucleus, facilitating DNA-binding and damaging followed by inducing tumor cell death.[36] Flow cytometry and CLSM results displayed that DOX@NPs could significantly promote DOX internalization in TNBC cells.

In vitro Cytotoxicity Assay

To further investigate the antitumor efficiency of different formulations, in vitro cell cytotoxicity was conducted in MDA-MB-231 and 4T1 cells using MTT assay.[37,38] Figure 6A shows decreased cell viability after free DOX and DOX@NPs treatment for 24 h and 48 h in a concentration-dependent manner. Free DOX showed significant antiproliferation effects to both tumor cells, which increased with prolonged incubation time. The entrapment of DOX into PGla-PPBP nanoparticles has shown improved inhibition than free DOX due to higher internalization efficiency. The 50% inhibitory concentration (IC_{50}) displayed a tendency like the data shown above (Table 2). Free DOX displayed a IC_{50} value of 7.258 and 3.785 μg/mL in MDA-MB-231 cells for 24 h and 48 h meanwhile that in 4T1 cells were 32.04 and 9.849 μg/mL, respectively. DOX@NPs could bring down the IC_{50} value for ~2-fold in MDA-MB-231 and 4T1 cells after 24 h incubation. IC_{50} results at 48 h display a similar tendency with that of 24 h incubation with DOX@NPs. These results were attributed to more efficient cellular internalization and ROS responsive drug release, resulting in higher cytotoxicity and reduced IC_{50} value.[39] Next, in vitro ROS generation of each sample in MDA-MB-231 and 4T1 cells was detected by the ROS kit. As shown in Figure 6B, there was no significant difference between control and DOX@NPs, indicating that the treatment of DOX@NPs did not have significant ROS generation capacity.[40,41] In order to assess the

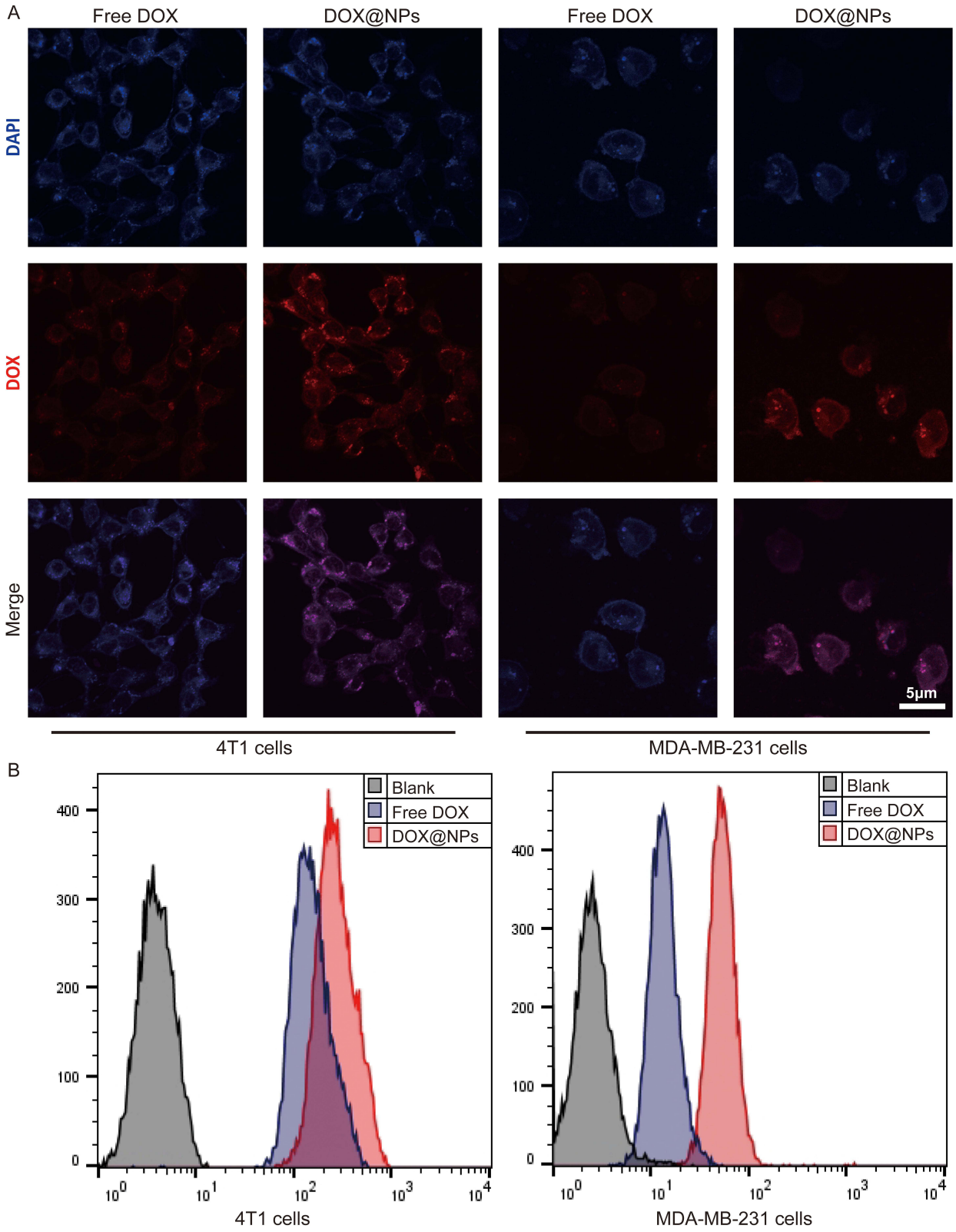

Figure 5 Cellular uptake of DOX@NPs in 4T1 cells and MDA-MB-231 cells. Tumor cells were incubated with free DOX or DOX@NPs for 4 h, and then analyzed by CLSM (**A**) and flow cytometry (**B**). Scale bar=5 μm.

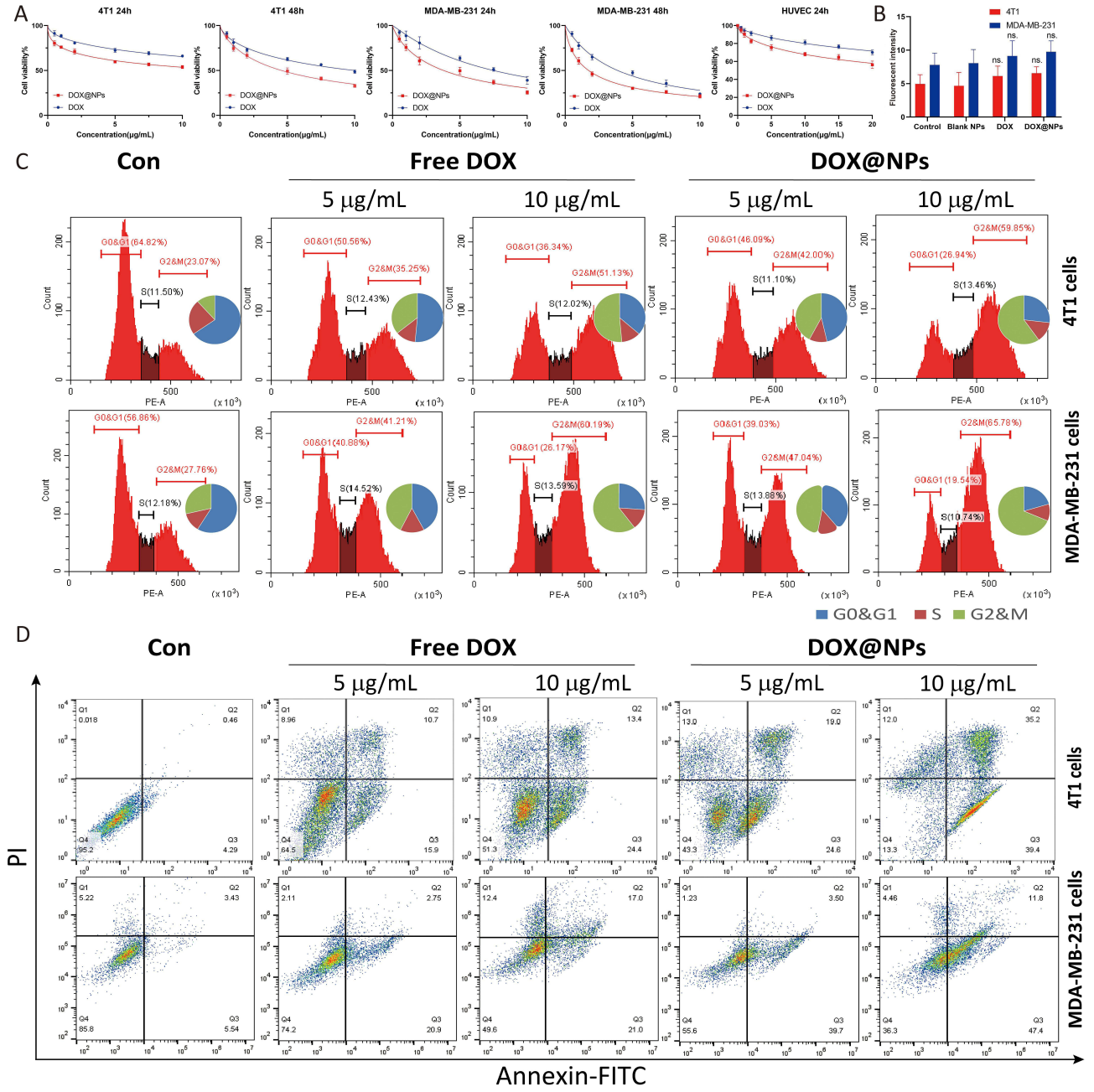

Figure 6 The cytotoxicity of different DOX formulations. (**A**) MTT assay was performed to evaluate the cytotoxicity of free DOX or DOX@NPs to 4T1, MDA-MB-231 and HUVEC cells. (**B**) In vitro ROS evaluation using DCFH-DA as ROS fluorescent probe in 4T1 and MDA-MB-231 cells. (Compared to control group, n=5) (**C**) 4T1 cells and MDA-MB-231 cells were incubated with 5–10 μg/mL free DOX or DOX@NPs for 12 h, and cell cycle assay was then analyzed by flow cytometry. (**D**) Apoptosis of tumor cells was analyzed by annexin V-FITC/PI staining after DOX@NPs (5 or 10 μg/mL) treatment.

toxic of DOX@NPs, HUVEC were used in this study. DOX@NPs-treatment resulted in weaker proliferation inhibition of HUVEC compared to 4T1 and MDA-MB-231 cells, verifying the low toxicity of DOX@NPs.

Cycle Arrest and Apoptosis Assay

The cell cycle distribution of MDA-MB-231 and 4T1 cells treated with free DOX and DOX@NPs micelles, at DOX concentration of 5 and 10 μg/mL, was analyzed by PI-staining measurement of DNA content using flow cytometry. As shown in Figure 6C, the obtain results showed that the percentage of MDA-MB-231 cells at G2/M stage were 27.76%, 41.21% (5 μg/mL) and 60.19% (10 μg/mL) after free DOX treatment. DOX@NPs yielded the higher percentage of cells

Table 2 IC_{50} Values of Tumor Cells Received Different Treatments (n=5)

		IC50 Values (μg/mL)	
		DOX	DOX@NPs
MDA-MB-231 cells	24 h	7.258	3.752
	48 h	3.785	1.695
4T1 cells	24 h	32.04	13.44
	48 h	9.849	4.461

in growth arrest compared to free DOX, which revealed 47.04% (5 μg/mL) and 65.78% (10 μg/mL) cells in G2/M stages. Moreover, the effect of DOX@NPs was accompanied with a reduction of the G0/G1 phase, with no significant impact in the S stage. Similar trends were also found in 4T1 cells, in which DOX@NPS enhanced the percentage (~18%) of cells in G2/M phase meanwhile reduced that in G0/G1 phase. The results proposed the improved cell cycle arrest of DOX@NPs at G2/M in both MDA-MB-231 and 4T1 cells.

Apoptosis, a pattern of programmed cell death, is one essential mechanism for most chemotherapeutic drug and nanomedicines.[36,39] We next investigated the effects of DOX@NPs on apoptosis using FITC-annexin V-PI staining by flow cytometry. As shown in Figure 6D, the total apoptosis (early and later apoptosis) of MDA-MB-231 cells induced by free DOX and DOX@NPs at 5 and 10 μg/mL affected 20.9%, 38.0%, 43.2%, and 58.8%, respectively, which was in line with cytotoxicity and cycle arrest assay. The prevalence of apoptosis of 4T1 cells after DOX@NPs (10 μg/mL) incubation was 74.6%, which was higher than that at 5 μg/mL (43.6%), and that induced by free DOX (26.6% and 37.4% for 5 and 10 μg/mL, respectively). These results suggested that the higher cytotoxicity, apoptosis and cell cycle arrest of DOX@NPs was attributed to higher internalization and intracellular ROS-triggered DOX release, which could efficiently inhibit TNBC cells.

In vivo Distribution

In vitro cellular uptake and cytotoxicity of DOX@NPs have been confirmed, which demonstrated efficient internalization and inhibition effect in MDA-MB-231 and 4T1 cells. To further evaluate tumor targeting, the biodistribution of DiR-labelled PGla-PPBP NPs was investigated using Premium Entry-level Optical Imaging (IVIS Lumina XRMS III, PerkinElmer, USA) after systemic administration. As shown in Figure 7, DiR fluorescence signal was observed in the liver at first 3 h and then mainly distributed in tumor site rather than other organs. Encouragingly, DiR distribution in the tumor region could be detected for more than 48 h, suggesting that the ROS-responsive nanocarrier could improve payload accumulation in tumor arising from passive targeting and ROS responsiveness. Ex vivo images further displayed tumor accumulation of DiR@NPs, suggesting that DOX@NPs could efficiently deliver DOX into the tumor as comparable sizes and zeta potential.

In vivo Antitumor Evaluation

Encouraged by improvements in vitro antitumor therapeutic efficacy and in vivo high tumor accumulation, tumor regression study of DOX@NPs was performed in a murine 4T1 tumor xenograft mice model. As shown in Figure 7, DOX@NPs were intravenously administrated into tumor-bearing mice every 2 days at a 4 mg/kg (L-DOX@NPs) and 8 mg/kg (H-DOX@NPs) dose, respectively.[38,42] After five consecutive injection of DOX formulations, the tumor growth was predominantly suppressed in comparison with saline group. DOX@NPs demonstrated better antitumor efficiency than free DOX ($P<0.05$). In the end of antitumor experiments, the tumor weight in saline group was 1.3- and 3.2-fold larger than that of free doxorubicin at 4 mg/kg and 8 mg/kg, respectively. Furthermore, the tumor weight of free DOX groups were 1.3-fold and 2.4-fold higher than that of DOX@NPs group at same concentrations, respectively. The representative optical tumor images further supported the potent tumor regression capability of DOX@NPs. These data suggested that DOX@NPs could efficiently inhibit tumor growth, which may be attributed to high tumor accumulation and ROS-responsive DOX release. In accordance with above results, H&E and Ki67 staining displayed that DOX@NPs

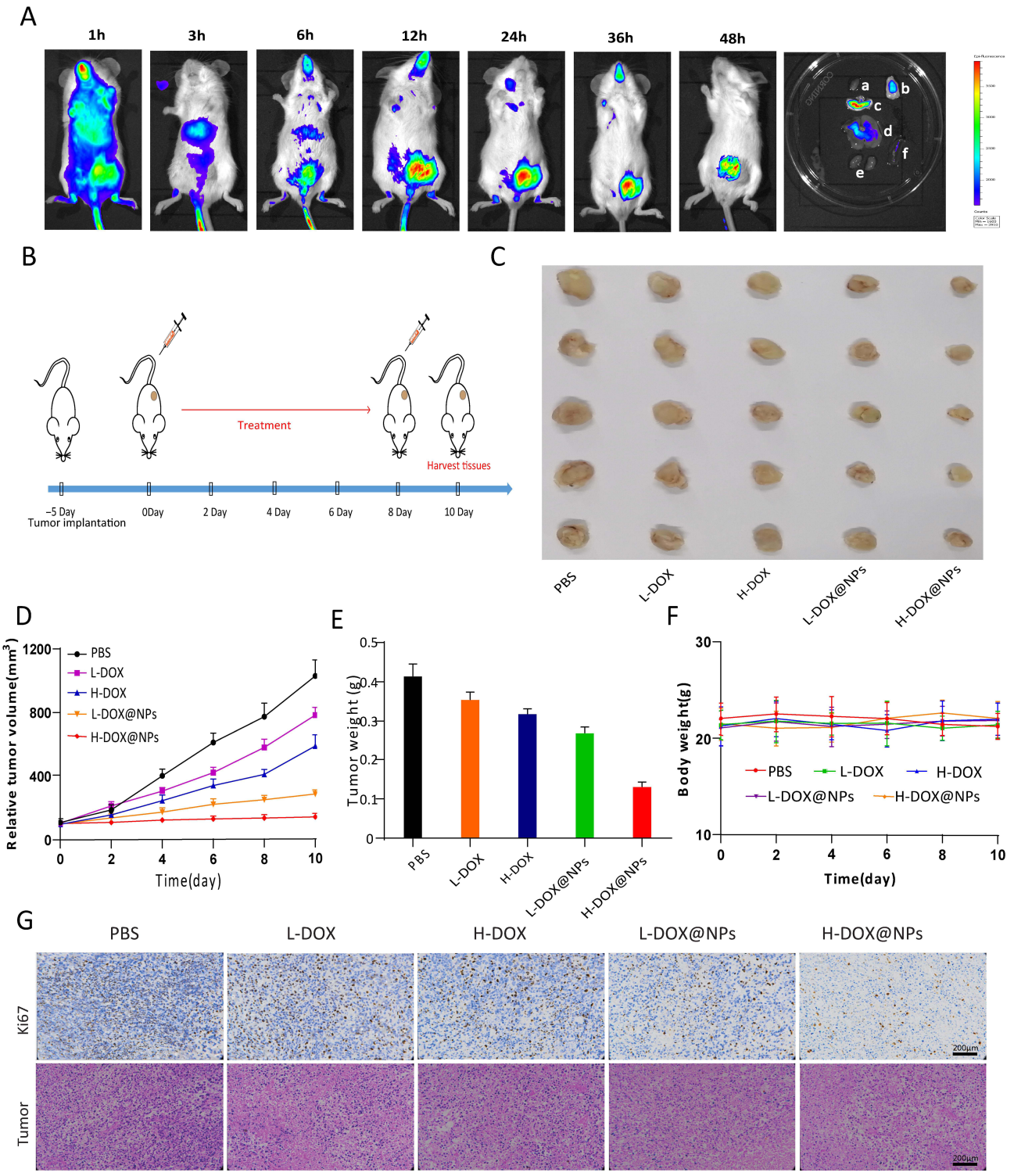

Figure 7 In vivo biodistribution and antitumor evaluation. (**A**) Fluorescence images of orthotopic 4T1 tumor-bearing Balb/c mice at different time points following intravenous injection of DiR@NPs (a: heart, b: tumor, c: lung, d: liver, e: kidney and f: spleen). (**B**) Therapeutic schedule for therapy. (**C**) Representative tumor images of the mice after different treatments for 10 days. (**D**) Tumor growth curves in 4T1 tumor-bearing mice after different DOX formulations treatments (n=5, mean ±SD). (**E**) Tumor weights of excised tumor tissues. Data was expressed as mean ±SD. (**F**) Variation in the body weight of the mice after different treatments. (**G**) H&E and Ki67 staining of 4T1 tumor tissues collected from mice after various treatments.

treatment had more favorable proapoptotic effects with extensive apoptotic and necrotic cells and reduced proliferation than free DOX group. All above results demonstrated that DOX@NPs could enable targeting drug delivery and efficient tumor suppression in TNBC therapy.

Safety Evaluation

Chemotherapeutic drugs have been reported to lead to serve damage to normal tissues.[43] Thus, histological changes in organs were investigated after DOX formulations treatment. For DOX, cardiac toxicity was the most common side effect. As shown in Figure 8A, damages to myocardium were observed for mice with 4–8 mg/kg five times. There were no obvious indications of toxicity obtained from mice treated with DOX@NPs, suggesting that the entrapment of DOX into nanoparticles decreased heart toxicity of DOX. Moreover, no significant differences were observed in other main organs such as the liver, spleen, lung and kidney that participate in the reticuloendothelial system and are considered as the major distribution sites for nanomedicines after intravenous administration. In this study, low and high DOX@NPs administration showed no significant abnormal changes in main organs compared to the PBS group, confirming the safety of DOX@NPs.

Furthermore, the toxicity in mice was monitored by serum chemistry examinations (Figure 8B–E). DOX triggers the disruption of cardiac myocytes and the release of intracellular CK into the serum.[44] CK of mice treated with free DOX were significantly higher compared to saline, indicating DOX-induced heart damage. The encapsulation of DOX obviously reduced the level of CK, which was associated with reduced biodistribution of nanoparticles in heart. In

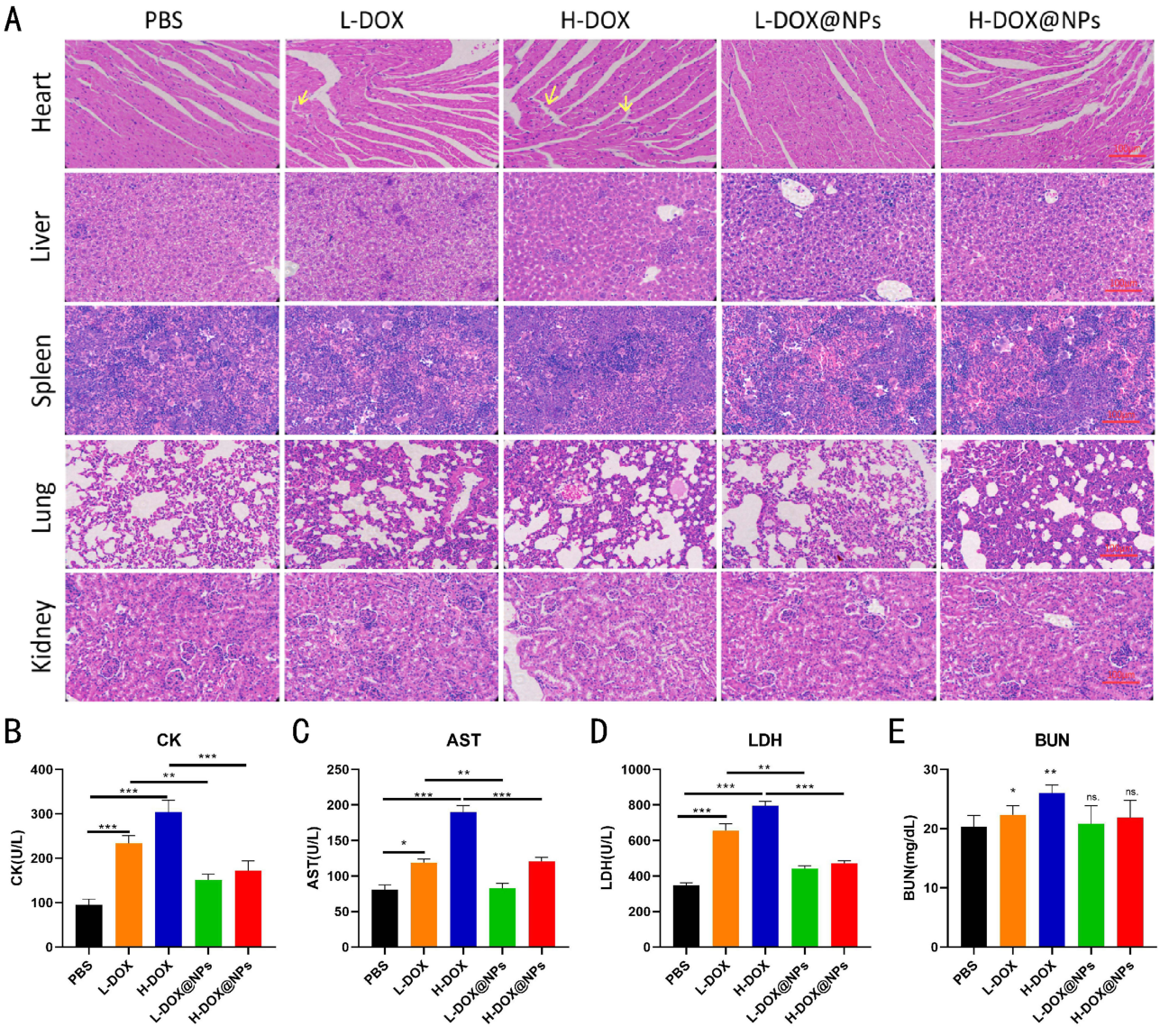

Figure 8 Safety evaluation. (**A**) H&E staining of main organs (hearts, livers, spleens, lungs, and kidneys) at the end of experiments. Yellow arrows represent damages to myocardium. Scale bar=100 μm. Hematological biochemical parameters of different formulations after treatment. (**B**–**E**) CK, AST, LDH, and BUN levels in different treatment groups. (Compared to control group. ns: $P>0.05$, *$P<0.05$, **$P<0.01$, ***$P<0.001$, n=5, mean ±SD).

addition, DOX@NPs treatment resulted in a significant decrease of AST, LDH, and BUN caused by the DOX. These results revealed that the DOX@NPs was safe and biocompatible, inducing no discernable side effects in vivo.

Conclusion

In conclusion, we developed ROS-responsive galactosylated nanoparticles with doxorubicin embedding for the treatment of TNBC. When DOX@NPs encountered intracellular ROS stimulation within tumor cells, the nanoparticles' structure was destroyed, resulting in intracellular DOX release, which resulted in apoptosis, cell cycle arrest, and death of tumor cells. In vivo, galactose modified nanoparticles demonstrated effective tumor accumulation, achieving targeted delivery of DOX and tumor suppression in 4T1 in situ breast cancer xenotransplantation. In this study, we used galactose selected as a hydrophilic segment, and since the galactose receptor is also highly expressed in liver cells, this strategy may also be applied to treating liver cancer and other cancers in future. However, the clinical translation of DOX@NPs is still challenging. The major limitations for their successful applications in breast cancer are need for elucidation of clearance mechanisms and lack of long-term studies (in vivo toxicity and antitumor evaluation).

Acknowledgment

We acknowledge financial support from National Natural Science Foundation of China (82003676).

Disclosure

The authors report no conflicts of interest in this work.

References

1. Khazaei-Poul Y, Shojaei S, Koochaki A, Ghanbarian H, Mohammadi-Yeganeh S. Evaluating the influence of human umbilical cord mesenchymal stem cells-derived exosomes loaded with miR-3182 on metastatic performance of triple negative breast cancer cells. *Life Sci*. 2021;286:120015. doi:10.1016/j.lfs.2021.120015
2. Haggag YA, Yasser M, Tambuwala MM, et al. Repurposing of Guanabenz acetate by encapsulation into long-circulating nanopolymersomes for treatment of triple-negative breast cancer. *Int J Pharm*. 2021;600:120532. doi:10.1016/j.ijpharm.2021.120532
3. Haggag Y, Abu Ras B, El-Tanani Y, et al. Co-delivery of a RanGTP inhibitory peptide and doxorubicin using dual-loaded liposomal carriers to combat chemotherapeutic resistance in breast cancer cells. *Expert Opin Drug Deliv*. 2020;17(11):1655–1669. doi:10.1080/17425247.2020.1813714
4. De Vita A, Liverani C, Molinaro R, et al. Lysyl oxidase engineered lipid nanovesicles for the treatment of triple negative breast cancer. *Sci Rep*. 2021;11(1):5107. doi:10.1038/s41598-021-84492-3
5. Zou T, Lan M, Liu F, et al. Emodin-loaded polymer-lipid hybrid nanoparticles enhance the sensitivity of breast cancer to doxorubicin by inhibiting epithelial–mesenchymal transition. *Cancer Nanotechnol*. 2021;12(1). doi:10.1186/s12645-021-00093-9
6. Liu J, Liu K, Zhang L, et al. Heat/pH-boosted release of 5-fluorouracil and albumin-bound paclitaxel from Cu-doped layered double hydroxide nanomedicine for synergistical chemo-photo-therapy of breast cancer. *J Control Release*. 2021;335:49–58. doi:10.1016/j.jconrel.2021.05.011
7. Molinaro R, Martinez JO, Zinger A, et al. Leukocyte-mimicking nanovesicles for effective doxorubicin delivery to treat breast cancer and melanoma. *Biomater Sci*. 2020;8(1):333–341. doi:10.1039/C9BM01766F
8. Alam W, Ullah H, Santarcangelo C, et al. Micronutrient food supplements in patients with gastro-intestinal and hepatic cancers. *Int J Mol Sci*. 2021;22(15):8014. doi:10.3390/ijms22158014
9. Peng F, Jeong S, Ho A, Evans CL. Recent progress in plasmonic nanoparticle-based biomarker detection and cytometry for the study of central nervous system disorders. *Cytometry A*. 2021;99(11):1067–1078. doi:10.1002/cyto.a.24489
10. Llop-Guevara A, Loibl S, Villacampa G, et al. Association of RAD51 with homologous recombination deficiency (HRD) and clinical outcomes in untreated triple-negative breast cancer (TNBC): analysis of the GeparSixto randomized clinical trial. *Ann Oncol*. 2021;32(12):1590–1596. doi:10.1016/j.annonc.2021.09.003
11. Girardi B, Manna M, Van Klaveren S, et al. Selective monovalent galectin-8 ligands based on 3-lactoylgalactoside. *Chem Med Chem*. 2022;17(3):e202100514.
12. Hesse C, Kollenda S, Rotan O, et al. A tumor-peptide-based nanoparticle vaccine elicits efficient tumor growth control in antitumor immunotherapy. *Mol Cancer Ther*. 2019;18(6):1069–1080. doi:10.1158/1535-7163.MCT-18-0764
13. Li C, Zhang D, Guo H, et al. Preparation and characterization of galactosylated bovine serum albumin nanoparticles for liver-targeted delivery of oridonin. *Int J Pharm*. 2013;448(1):79–86. doi:10.1016/j.ijpharm.2013.03.019
14. Qiu L, Li Z, Qiao M, et al. Self-assembled pH-responsive hyaluronic acid-g-poly((L)-histidine) copolymer micelles for targeted intracellular delivery of doxorubicin. *Acta Biomater*. 2014;10(5):2024–2035. doi:10.1016/j.actbio.2013.12.025
15. Chen Q, Long M, Qiu L, et al. Decoration of pH-sensitive copolymer micelles with tumor-specific peptide for enhanced cellular uptake of doxorubicin. *Int J Nanomedicine*. 2016;11:5415–5427. doi:10.2147/IJN.S111950
16. Li K, Zang X, Cheng M, Chen X. Stimuli-responsive nanoparticles based on poly acrylic derivatives for tumor therapy. *Int J Pharm*. 2021;601:120506. doi:10.1016/j.ijpharm.2021.120506
17. Piloni A, Wong CK, Chen F, et al. Surface roughness influences the protein Corona formation of glycosylated nanoparticles and alter their cellular uptake. *Nanoscale*. 2019;11(48):23259–23267. doi:10.1039/C9NR06835J

18. Zheng M, Liu Y, Wang Y, et al. ROS-responsive polymeric siRNA nanomedicine stabilized by triple interactions for the robust glioblastoma combinational RNAi therapy. *Adv Mater*. 2019;31(37):e1903277. doi:10.1002/adma.201903277
19. Yu Y, Chen J, Liu S, Cheng D. ROS-responsive organosilica nanocarrier for the targeted delivery of metformin against cancer with the synergistic effect of hypoglycemia. *J Mater Chem B*. 2021;9(30):6044–6055. doi:10.1039/D1TB01143J
20. Pei Y, Li M, Hou Y, et al. An autonomous tumor-targeted nanoprodrug for reactive oxygen species-activatable dual-cytochrome c/doxorubicin antitumor therapy. *Nanoscale*. 2018;10(24):11418–11429. doi:10.1039/C8NR02358A
21. Shao J, Liang R, Ding D, Zheng X, Zhu X, Hu S, Wei H and Wei B. (2021). A Smart Multifunctional Nanoparticle for Enhanced Near-Infrared Image-Guided Photothermal Therapy Against Gastric Cancer. IJN, Volume 16 2897–2915. doi:10.2147/IJN.S289310
22. Ahmadi M, Siavashy S, Ayyoubzadeh SM, Kecili R, Ghorbani-Bidkorbeh F. Controllable synthesis of polymeric micelles by microfluidic platforms for biomedical applications: a systematic review. *Iran J Pharm Res*. 2021;20(2):229–240. doi:10.22037/ijpr.2021.114226.14769
23. Alfei S, Brullo C, Caviglia D, Zuccari G. Preparation and physicochemical characterization of water-soluble pyrazole-based nanoparticles by dendrimer encapsulation of an insoluble bioactive pyrazole derivative. *Nanomaterials*. 2021;11(10):2662. doi:10.3390/nano11102662
24. Tieu T, Wojnilowicz M, Huda P, et al. Nanobody-displaying porous silicon nanoparticles for the co-delivery of siRNA and doxorubicin. *Biomater Sci*. 2021;9(1):133–147. doi:10.1039/D0BM01335H
25. Oddone N, Pederzoli F, Duskey JT, et al. ROS-responsive "smart" polymeric conjugate: synthesis, characterization and proof-of-concept study. *Int J Pharm*. 2019;570:118655. doi:10.1016/j.ijpharm.2019.118655
26. Hayward SW. Immunotherapeutic response in tumors is affected by microenvironmental ROS. *Cancer Res*. 2020;80(9):1799–1800. doi:10.1158/0008-5472.CAN-20-0590
27. Luo Z, Wang C, Yi H, et al. Nanovaccine loaded with poly I:C and STAT3 siRNA robustly elicits anti-tumor immune responses through modulating tumor-associated dendritic cells in vivo. *Biomaterials*. 2015;38:50–60. doi:10.1016/j.biomaterials.2014.10.050
28. Fang G, Lu H, Al-Nakashli R, et al. Enabling peristalsis of human colon tumor organoids on microfluidic chips. *Biofabrication*. 2021;14(1). doi:10.1088/1758-5090/ac2ef9
29. Abuhamdan RM, Al-Anati BH, Al Thaher Y, et al. Aqueous core microcapsules as potential long-acting release systems for hydrophilic drugs. *Int J Pharm*. 2021;606:120926. doi:10.1016/j.ijpharm.2021.120926
30. Alves PGV, de Paula Menezes R, de Oliveira Brito M, et al. Cryptococcus liquefaciens isolated from the hand of a healthcare professional in a neonatal intensive care unit. *Braz J Microbiol*. 2021;52(4):2085–2089. doi:10.1007/s42770-021-00601-4
31. de Oliveira Pedro R, Goycoolea FM, Pereira S, Schmitt CC, Neumann MG. Synergistic effect of quercetin and pH-responsive DEAE-chitosan carriers as drug delivery system for breast cancer treatment. *Int J Biol Macromol*. 2018;106:579–586. doi:10.1016/j.ijbiomac.2017.08.056
32. Bonferoni MC, Rassu G, Gavini E, et al. Electrochemotherapy of deep-seated tumors: state of art and perspectives as possible "EPR effect enhancer" to improve cancer nanomedicine efficacy. *Cancers*. 2021;13(17):4437. doi:10.3390/cancers13174437
33. Gao L, Teng R, Zhang S, et al. Zinc Ion-stabilized aptamer-targeted black phosphorus nanosheets for enhanced photothermal/chemotherapy against prostate cancer. *Front Bioeng Biotechnol*. 2020;8:769. doi:10.3389/fbioe.2020.00769
34. Marulanda K, Mercel A, Gillis DC, et al. Intravenous delivery of lung-targeted nanofibers for pulmonary hypertension in mice. *Adv Healthc Mater*. 2021;10(13):e2100302. doi:10.1002/adhm.202100302
35. Yan J, Zhang N, Zhang Z, et al. Redox-responsive polyethyleneimine/tetrahedron DNA/doxorubicin nanocomplexes for deep cell/tissue penetration to overcome multidrug resistance. *J Control Release*. 2021;329:36–49. doi:10.1016/j.jconrel.2020.11.050
36. Yang J, Li Q, Zhou M, et al. Concurrent impairment of nucleus and mitochondria for synergistic inhibition of cancer metastasis. *Int J Pharm*. 2021;608:121077. doi:10.1016/j.ijpharm.2021.121077
37. Gupta B, Poudel BK, Ruttala HB, et al. Hyaluronic acid-capped compact silica-supported mesoporous titania nanoparticles for ligand-directed delivery of doxorubicin. *Acta Biomater*. 2018;80:364–377. doi:10.1016/j.actbio.2018.09.006
38. Chen K, Cai H, Zhang H, et al. Stimuli-responsive polymer-doxorubicin conjugate: antitumor mechanism and potential as nano-prodrug. *Acta Biomater*. 2019;84:339–355. doi:10.1016/j.actbio.2018.11.050
39. Tang D, Wang Y, Wijaya A, et al. ROS-responsive biomimetic nanoparticles for potential application in targeted anti-atherosclerosis. *Regen Biomater*. 2021;8(4):rbab033. doi:10.1093/rb/rbab033
40. Zhou Z, Wang C, Bai J, et al. Cinnamaldehyde-modified chitosan hybrid nanoparticles for DOX delivering to produce synergistic anti-tumor effects. *Front Bioeng Biotechnol*. 2022;10:968065. doi:10.3389/fbioe.2022.968065
41. Ding Y, Wang C, Ma Y, et al. Tumor microenvironment responsive polypeptide-based supramolecular nanoprodrugs for combination therapy. *Acta Biomater*. 2022;146:396–405. doi:10.1016/j.actbio.2022.04.027
42. Ren G, Duan D, Wang G, et al. Construction of reduction-sensitive heterodimer prodrugs of doxorubicin and dihydroartemisinin self-assembled nanoparticles with antitumor activity. *Colloids Surf B Biointerfaces*. 2022;217:112614. doi:10.1016/j.colsurfb.2022.112614
43. Yu JJ, Lee HA, Kim JH, et al. Bio-distribution and anti-tumor efficacy of PEG/PLA nano particles loaded doxorubicin. *J Drug Target*. 2007;15(4):279–284. doi:10.1080/10611860701357235
44. DeAtley SM, Aksenov MY, Aksenova MV, et al. Adriamycin-induced changes of creatine kinase activity in vivo and in cardiomyocyte culture. *Toxicology*. 1999;134(1):51–62. doi:10.1016/S0300-483X(99)00039-6